

Graphical Abstract

A Linear Quadratic Integral Differential Game Approach for Attitude Control of an Experimental Platform of a Quadrotor

Hadi Nobahari, Ali BaniAsad, Reza Pordal, Alireza Sharifi

A Linear Quadratic Integral Differential Game Approach for Attitude Control of an Experimental Platform of a Quadrotor

Hadi Nobahari, Ali BaniAsad, Reza Pordal, Alireza Sharifi

^a*Department of Aerospace Engineering Sharif University of Technology, Tehran, Iran*

Abstract

This research paper presents a novel approach to quadrotor attitude control that draws on differential game theory. The approach uses a linear quadratic Gaussian (LQG) controller with integral actions. Accurate attitude control is of utmost importance for safe and effective quadrotor flight, particularly in the presence of disturbances. To develop a dependable and effective control system, the motion equations with nonlinearity for the quadrotor's experimental setup are transformed into a continuous-time state-space model through linearization. Experimental data are used to identify model parameters, and attitude control commands are determined using two-player approaches. By mini-maximizing a quadratic set of criteria, which is the total of the outputs and disturbances weighted by the amount of control effort, one player minimizes the command while the other generates disturbances. The performance of the proposed approach is evaluated by comparing it to a linear quadratic regulator controller in level flight. The results demonstrate that the proposed approach effectively dissipates disturbances and outperforms linear quadratic regulator controllers, thereby contributing to the development of robust and effective attitude control systems for quadrotors.

Keywords:

Linear quadratic Gaussian controller, Differential game theory, Quadrotor, Continuous state-space model, three-degree-of-freedom experimental platform, Attitude Control Optimization, Robust disturbance rejection.

Email addresses: nobahari@sharif.edu (Hadi Nobahari),
ali.baniasad@ae.sharif.edu (Ali BaniAsad), email address (Reza Pordal),
alireza_sharifi@ae.sharif.edu (Alireza Sharifi)

1. Introduction

The investigation, strategic operations, optical sensing, entertainment, and farming are all used by quadrotors in today's society (Fathoni et al., 2021).

2. Problem Formulation

The experimental quadrotor platform rotates freely with rotational velocity about its roll, pitch, and yaw axes, as shown in Figure 1. The Euler angles and their derivatives are measured using an Attitude Heading Reference System (AHRS), which is utilized in the structure of the LQIR-DG controller to stabilize the quadrotor platform. The graphical representation of the proposed controller structure is depicted in Figure 2.



Figure 1: 3DoF setup of the quadrotor.

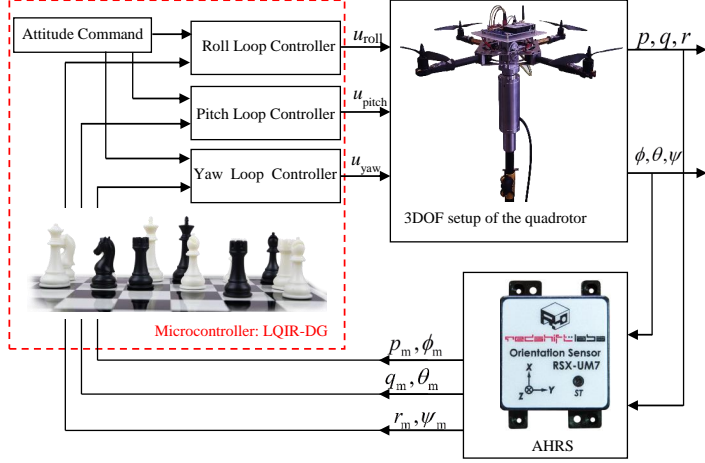


Figure 2: Structure of the LQIG-DG Controller Illustrated in a Block Diagram.

3. Dynamic Model of the Quadrotor Platform

In this section, first, a nonlinear model for the quadrotor platform is derived. Then, a state-space model and a linear model are developed for control purposes to be utilized in a controller strategy. Finally, a nonlinear identification method is applied to identify the parameters of the quadrotor.

3.1. Quadrotor Configuration

Figure 3 shows the quadrotor schematic. It depicts four rotors rotating around the z_B axis in the coordinate system of the body. The rotors have a rotational velocity of Ω_r . The quadrotor platform has 3 degrees of freedom, including roll, pitch, and yaw motions, which are described by roll (ϕ), pitch (θ), and yaw (ψ) angles, respectively. The counterclockwise rotation of Rotors 1 and 3 generates a moment that counteracts the yawing moment, while the clockwise rotation of Rotors 2 and 4 produces a moment that also counteracts the yawing moment.

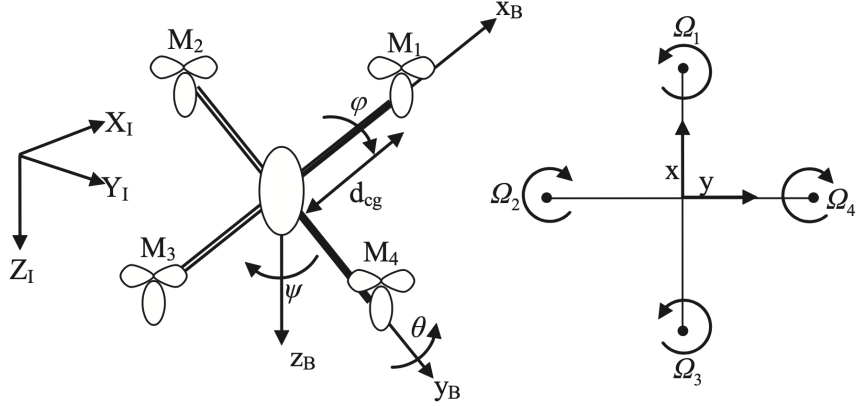


Figure 3: Quadrotor Configuration.

3.2. Dynamic Modeling of the Quadrotor Platform

Here, according to Newton-Euler, the dynamic model of the quadrotor platform is derived as follows Bouabdallah and Siegwart (2007); Bouabdallah (2007):

$$\dot{p} = \frac{I_{yy} - I_{zz}}{I_{xx}} qr + q \frac{I_{rotor}}{I_{xx}} \Omega_r + \frac{u_{roll}}{I_{xx}} + \frac{d_{roll}}{I_{xx}} \quad (1)$$

$$\dot{q} = \frac{I_{zz} - I_{xx}}{I_{yy}} rp + p \frac{I_{rotor}}{I_{xx}} \Omega_r + \frac{u_{pitch}}{I_{yy}} + \frac{d_{pitch}}{I_{yy}} \quad (2)$$

$$\dot{r} = \frac{I_{xx} - I_{yy}}{I_{zz}} pq + \frac{u_{yaw}}{I_{zz}} + \frac{d_{yaw}}{I_{zz}} \quad (3)$$

The (p, q, r) represent the rotational variables, and d_{roll} , d_{pitch} , and d_{yaw} denote the disturbances produced in the x_B , y_B , and z_B axes, respectively. Additionally, I_{xx} , I_{yy} , and I_{zz} are the principal moments of inertia, and I_{rotor} is the rotor inertia about its axis. Euler angle rates are also determined from angular body rates as follows:

$$\begin{bmatrix} \dot{\phi} \\ \dot{\theta} \\ \dot{\psi} \end{bmatrix} \begin{bmatrix} 1 & \sin(\phi) \tan(\theta) & \cos(\phi) \tan(\theta) \\ 0 & \cos(\phi) & -\sin(\phi) \\ 0 & \sin(\phi)/\cos(\theta) & \cos(\phi)/\cos(\theta) \end{bmatrix} \begin{bmatrix} p \\ q \\ r \end{bmatrix} \quad (4)$$

The residual rotor velocity, denoted by Ω_r , is calculated as follows:

$$\Omega_r = -\Omega_1 + \Omega_2 - \Omega_3 + \Omega_4 \quad (5)$$

3.3. Input of the Dynamic Model

The control inputs u_{roll} , u_{pitch} , and u_{yaw} are to the moments generated by the quadrotor's rotors along the roll, pitch, and yaw axes, respectively, defined as follows:

$$u_{\text{roll}} = b d_{\text{cg}} (\Omega_2^2 - \Omega_4^2) \quad (6)$$

$$u_{\text{pitch}} = b d_{\text{cg}} (\Omega_1^2 - \Omega_3^2) \quad (7)$$

$$u_{\text{yaw}} = d (\Omega_1^2 - \Omega_2^2 + \Omega_3^2 - \Omega_4^2) \quad (8)$$

where d_{cg} , d , and b represent the distance between the rotors and the gravity center, drag factor, and thrust factor, respectively. The rotational velocity commands are computed as follows:

$$\Omega_{c,1}^2 = \Omega_{\text{mean}}^2 + \frac{1}{2b d_{\text{cg}}} u_{\text{pitch}} + \frac{1}{4d} u_{\text{yaw}} \quad (9)$$

$$\Omega_{c,2}^2 = \Omega_{\text{mean}}^2 + \frac{1}{2b d_{\text{cg}}} u_{\text{roll}} - \frac{1}{4d} u_{\text{yaw}} \quad (10)$$

$$\Omega_{c,3}^2 = \Omega_{\text{mean}}^2 - \frac{1}{2b d_{\text{cg}}} u_{\text{pitch}} + \frac{1}{4d} u_{\text{yaw}} \quad (11)$$

$$\Omega_{c,4}^2 = \Omega_{\text{mean}}^2 - \frac{1}{2b d_{\text{cg}}} u_{\text{roll}} - \frac{1}{4d} u_{\text{yaw}} \quad (12)$$

In the above equation, Ω_{mean} is nominal rotational velocities of the rotors.

3.4. State-Space Formulation

Here, by defining $x_1 = p$, $x_2 = q$, $x_3 = r$, $x_4 = \phi$, $x_5 = \theta$, and $x_6 = \psi$, the formulation of the quadrotor platform is presented as follows:

$$\dot{x}_1 = \Gamma_1 x_2 x_3 + \Gamma_2 x_2 \Omega_r + \Gamma_3 u_{\text{roll}} + \Gamma_3 d_{\text{roll}} \quad (13)$$

$$\dot{x}_2 = \Gamma_4 x_1 x_3 - \Gamma_5 x_1 \Omega_r + \Gamma_6 u_{\text{pitch}} + \Gamma_6 d_{\text{pitch}} \quad (14)$$

$$\dot{x}_3 = \Gamma_7 x_1 x_2 + \Gamma_8 u_{\text{yaw}} + \Gamma_8 d_{\text{yaw}} \quad (15)$$

$$\dot{x}_4 = x_1 + (x_2 \sin(x_4) + x_3 \cos(x_4)) \tan(x_5) \quad (16)$$

$$\dot{x}_5 = x_2 \cos(x_4) - x_3 \sin(x_4) \quad (17)$$

$$\dot{x}_6 = (x_2 \sin(x_4) + x_3 \cos(x_4)) / \cos(x_5) \quad (18)$$

where $\Gamma_i (i = 1, \dots, 8)$ is defined as:

$$\begin{aligned}\Gamma_1 &= \frac{I_{yy} - I_{zz}}{I_{xx}}, & \Gamma_2 &= \frac{I_{\text{rotor}}}{I_{xx}}, & \Gamma_3 &= \frac{1}{I_{xx}} \\ \Gamma_4 &= \frac{I_{zz} - I_{xx}}{I_{yy}}, & \Gamma_5 &= \frac{I_{\text{rotor}}}{I_{yy}}, & \Gamma_6 &= \frac{1}{I_{yy}} \\ \Gamma_7 &= \frac{I_{xx} - I_{yy}}{I_{zz}}, & \Gamma_8 &= \frac{1}{I_{zz}}\end{aligned}\quad (19)$$

Moreover, the measurement vector, obtained from the AHRS sensor is presented as follows:

$$\mathbf{z} = [p \ q \ r \ \phi \ \theta \ \psi]^T + \boldsymbol{\nu} \quad (20)$$

where $\boldsymbol{\nu}$ is a Gaussian white noise. In the above equation, the superscripts T indicate the transpose notation.

3.5. Linear Model

The linear continuous-time model of the quadrotor platform about the equilibrium points ($\mathbf{x}_e \neq 0$ and $\mathbf{u}_e \neq 0$) is represented as:

$$\dot{\mathbf{x}}(t) = \mathbf{A} \mathbf{x}(t) + \mathbf{B} \mathbf{u}(t) + \mathbf{B}_d \mathbf{d}(t) \quad (21)$$

where $\dot{\mathbf{x}} = [\dot{\mathbf{x}}_{\text{roll}} \ \dot{\mathbf{x}}_{\text{pitch}} \ \dot{\mathbf{x}}_{\text{yaw}}]$, defined as:

$$\mathbf{x}_{\text{roll}} = \begin{bmatrix} p \\ \phi \end{bmatrix}, \quad \mathbf{x}_{\text{pitch}} = \begin{bmatrix} q \\ \theta \end{bmatrix}, \quad \mathbf{x}_{\text{yaw}} = \begin{bmatrix} r \\ \psi \end{bmatrix} \quad (22)$$

Moreover, \mathbf{B} and \mathbf{B}_d are the input and disturbance matrices, respectively, and are defined as:

$$\mathbf{B} = \mathbf{B}_d = \begin{bmatrix} \mathbf{B}_{\text{roll}} & \mathbf{0} & \mathbf{0} \\ \mathbf{0} & \mathbf{B}_{\text{pitch}} & \mathbf{0} \\ \mathbf{0} & \mathbf{0} & \mathbf{B}_{\text{yaw}} \end{bmatrix} \quad (23)$$

In addition, the input matrices and state are shown as:

$$\mathbf{A}_{\text{roll}} = \mathbf{A}_{\text{pitch}} = \mathbf{A}_{\text{yaw}} = \begin{bmatrix} 0 & 0 \\ 1 & 0 \end{bmatrix} \quad (24)$$

$$\mathbf{B}_{\text{roll}} = \begin{bmatrix} 1 \\ \overline{I_{xx}} \\ 0 \end{bmatrix}; \quad \mathbf{B}_{\text{pitch}} = \begin{bmatrix} 1 \\ \overline{I_{yy}} \\ 0 \end{bmatrix}; \quad \mathbf{B}_{\text{yaw}} = \begin{bmatrix} 1 \\ \overline{I_{zz}} \\ 0 \end{bmatrix} \quad (25)$$

3.6. Identification of the Platform Parameters

This section describes the utilization of the Nonlinear Least Squares (NLS) algorithm for estimating the model parameters (Γ) of the 3DoF experimental platform using experimental data. This technique is based on the Trust-Region Reflective Least Squares (TRRLS) method, which iteratively finds the values of the model parameters by minimizing a cost function, defined as follows:

$$\min_{\Gamma_i} (\| e(\Gamma_i) \|^2) = \min_{\Gamma_i} = \left(\sum_{j=1}^n (\mathbf{z}_j - \hat{\mathbf{z}}_j)(\mathbf{z}_j - \hat{\mathbf{z}}_j)^T \right) \quad (26)$$

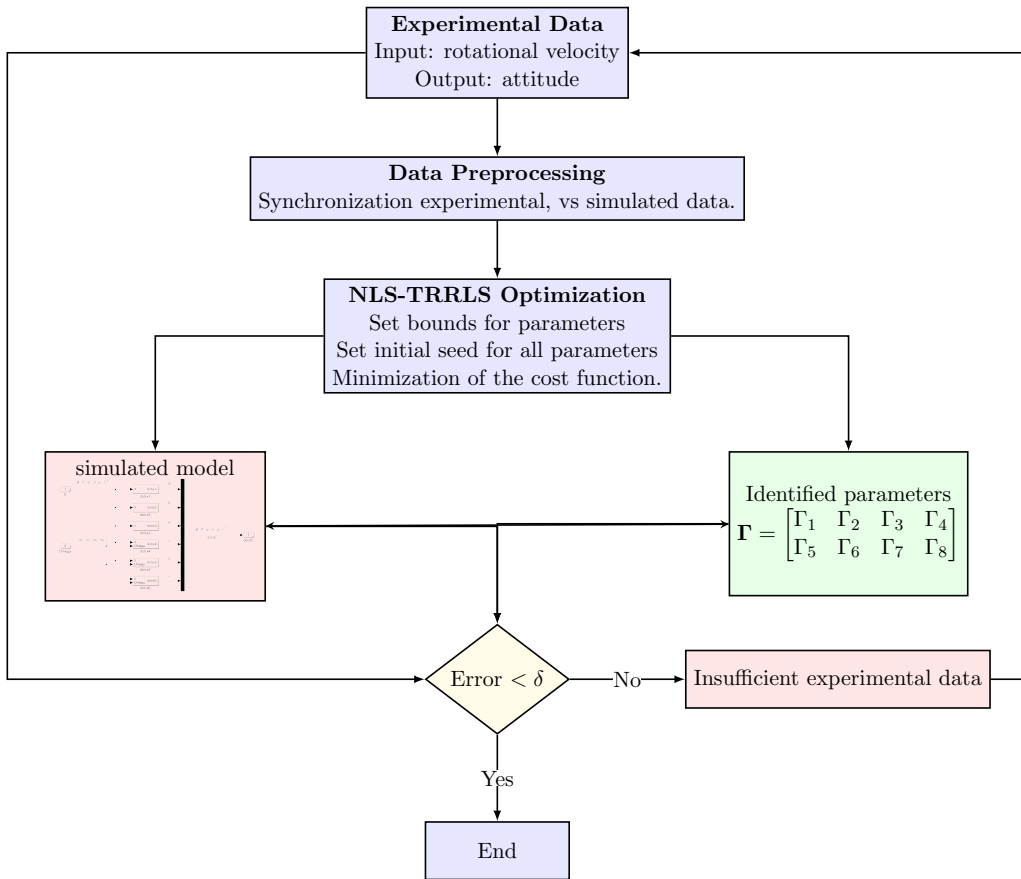


Figure 4: Structure of TRRLS identification approach.

4. Formulation of the LQDG Controller

Here, the LQR-DG controller is augmented with an integral action to eliminate steady-state errors. For this purpose, the augmented states of the quadrotor platform, which include states and their integrals, are selected. The design methodology of the LQR-DG controller is introduced. It generates optimal control signals for the three degrees of freedom platform.

4.1. Augmented State Space Development

To integrate the integrator into the control strategy architecture, the augmented state variables are defined below:

$$\mathbf{x}_{\mathbf{a}_i} = \begin{bmatrix} \mathbf{x}_i \\ \int \mathbf{x}_i \end{bmatrix} \quad (27)$$

The dynamics model of the quadrotor, as expressed by Eq. (21), is reformulated into an augmented state-space model that incorporates the roll (ϕ), pitch (θ), and yaw (ψ) angles. The augmented state-space model provides a comprehensive description of the quadrotor's dynamic behavior, enabling the design of effective control strategies. The ensuing state-space model that integrates the augmented state variables is mathematically represented and defined in the following manner:

$$\dot{\mathbf{x}}_a(t) = \mathbf{A}_a \mathbf{x}_a(t) + \mathbf{B}_a \mathbf{u}(t) + \mathbf{B}_{d_a} \mathbf{d}(t) \quad (28)$$

\mathbf{B}_a and \mathbf{A}_a , which are expressed as below:

$$\mathbf{B}_a = \mathbf{B}_{d_a} = \begin{bmatrix} \mathbf{B} \\ \mathbf{0} \end{bmatrix} \quad (29)$$

$$\mathbf{A}_a = \begin{bmatrix} \mathbf{A} & \mathbf{0} \\ \mathbf{I} & \mathbf{0} \end{bmatrix} \quad (30)$$

In the aforementioned expression, the notation \mathbf{I} denotes the identity matrix.

4.2. LQR-DG Control Scheme with Integral Action

In line with the principles of differential game theory, the LQIR-DG controller is designed to be both robust and optimal. The LQIR-DG scheme involves selecting two fundamental players, one responsible for determining the control command and the other for generating the worst possible disturbance. To achieve the primary objective, the primary player minimizes the following cost function, while the other player must maximize it:

$$\min_u \max_d J(\mathbf{x}_{\mathbf{a}_i}, d_i, u_i) = J(\mathbf{x}_{\mathbf{a}_i}, u_i^*, d_i^*) = \min_d \max_u \int_0^{t_f} \left(\mathbf{x}_{\mathbf{a}_i}^T \mathbf{Q}_i \mathbf{x}_{\mathbf{a}_i} + u_i^T R u_i - d_i^T R_d d_i \right) dt \quad (31)$$

where \mathbf{Q}_i , R_d , and R are weight coefficients of the function. The final time is denoted by t_f . By solving the above problem, the control command is computed as follows Engwerda (2006):

$$d_i(t) = \mathbf{K}_{d_i}(t) \mathbf{x}_{\mathbf{a}_i}(t) \quad (32)$$

Moreover, the worst disturbance is obtained as:

$$u_i(t) = -\mathbf{K}_i(t) \mathbf{x}_{\mathbf{a}_i}(t) \quad (33)$$

Here, \mathbf{K}_{d_i} and \mathbf{K}_i are gain values defined as follows:

$$\mathbf{K}_i = R^{-1} \mathbf{B}_{a_i}^T \mathbf{P}_{a_i}(t) \quad (34)$$

$$\mathbf{K}_{d_i} = R_d^{-1} \mathbf{B}_{a_{d_i}}^T \mathbf{P}_{a_{d_i}}(t) \quad (35)$$

where $\mathbf{P}_{a_i}(t)$ and $\mathbf{P}_{a_{d_i}}(t)$ satisfy

$$-\mathbf{A}_a^T \mathbf{P}_{a_{d_i}}(t) - \mathbf{Q}_i - \mathbf{P}_{a_{d_i}}(t) \mathbf{A}_a + \mathbf{P}_{a_{d_i}}(t) \mathbf{S}_{a_i}(t) \mathbf{P}_{a_i}(t) + \mathbf{P}_{a_{d_i}}(t) \mathbf{S}_{a_{d_i}}(t) \mathbf{P}_{a_{d_i}}(t) = \mathbf{0} \quad (36)$$

$$-\mathbf{A}_a^T \mathbf{P}_{a_i}(t) - \mathbf{Q}_i - \mathbf{P}_{a_i}(t) \mathbf{A}_a + \mathbf{P}_{a_i}(t) \mathbf{S}_{a_{d_i}}(t) \mathbf{P}_{a_{d_i}}(t) + \mathbf{P}_{a_i}(t) \mathbf{S}_{a_i}(t) \mathbf{P}_{a_i}(t) = \mathbf{0} \quad (37)$$

where

$$\mathbf{S}_{a_i} = \mathbf{B}_{a_i} R^{-1} \mathbf{B}_{a_i}^T, \quad \mathbf{S}_{a_{d_i}} = \mathbf{B}_{a_{d_i}} R_d^{-1} \mathbf{B}_{a_{d_i}}^T$$

5. Result and Discussion

Here, the simulation results of parameter identification and LQIDG-Controller for a quadrotor platform are presented. First, the quadrotor parameters are estimated based on the NLS method. Then, the performance of the LQDG controller structure is evaluated. The performance of the quadrotor LQIDG controller is presented in Tables 1 and 2.

Table 1: Quadrotor Parameters

Parameter	Value	Unit
d_{cg}	0.2	m
d	3.2×10^{-6}	N.m.sec ² /rad ²
b	3.13×10^{-5}	N.sec ² /rad ²
I_{xx}	0.02839	kg.m ²
I_{yy}	0.03066	kg.m ²
I_{zz}	0.0439	kg.m ²
I_{rotor}	4.4398×10^{-5}	kg.m ²
Ω_{mean}	3000	rpm

Table 2: LQIR-DG Controller Parameters

Channel	Weighting Matrix	Matrix Values
Roll	Q_{roll}	diag([0.02, 65.96, 83.04, 0.00])
Pitch	Q_{pitch}	diag([435.01, 262.60, 262.60, 0.00])
Yaw	Q_{yaw}	diag([4×10^{-4} , 0.00, 0.133, 0])
	R	1
	R_d	1.2764

5.1. Identification of the 3DoF quadrotor platform model

As described in section 3.4, the parameters of the quadrotor platform, denoted by $\Gamma_i (i = 1, \dots, 8)$, are identified using the NRS algorithm. The NLS-

TRRLS algorithm is implemented in Matlab R2022b®. To increase the accuracy of parameter identification, three scenarios according to Table 3. In the first scenario, depicted in Figure 5, the quadrotor is rotated about only one axis (roll, pitch, or yaw axes) to identify the parameters Γ_3 , Γ_6 , and Γ_8 . In the second scenario, as illustrated in Figure 6, the parameters Γ_2 and Γ_5 are estimated by moving the experimental platform to freely rotate around its roll and pitch axes simultaneously. When the stopping condition of the NLS algorithm is met, the optimal values of the quadrotor parameters are computed and presented in Table 4. These results illustrate that the outputs of the simulation results for the quadrotor model are consistent with reality.

Table 3: Scenarios for Identification of Quadrotor Parameters.

Scenario	<i>Description</i>	<i>Initial Condition (deg)</i>			<i>Rotational Velocity Commands</i>			
		ϕ	θ	ψ	Ω_1	Ω_2	Ω_3	Ω_4
I	Roll free	38	-	-	2000	2000	2000	3400
	Pitch free	-	-15	-	3700	2000	2000	2000
	Yaw free	-	-	-75	2000	3300	2000	3300
II	Roll and Pitch free	8	-5	-	1700	3800	2400	1700
III	Roll, Pitch, and Yaw free	8	-3	-146	1700	3800	2400	1700

Table 4: True values of the quadrotor parameters.

Parameter	Value	Parameter	Value
Γ_1	-0.9622	Γ_5	3.6441×10^{-4}
Γ_2	-0.0154	Γ_6	7.5395×10^{-5}
Γ_3	5.4716×10^{-5}	Γ_7	0.1308
Γ_4	1.0457	Γ_8	4.3753×10^{-5}

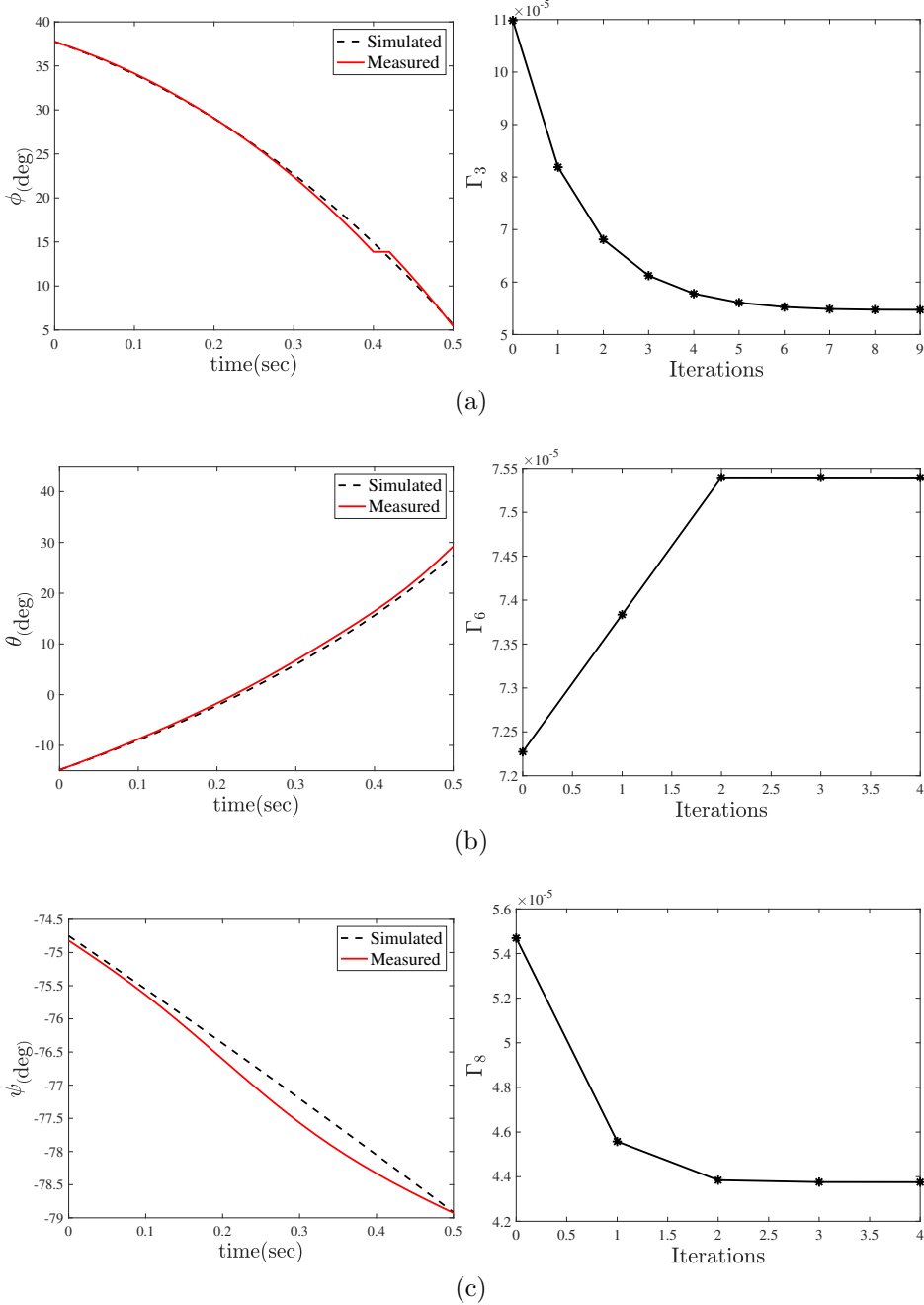


Figure 5: Identification process results when the quadrotor rotates about only one axis:
 (a) Identification of Γ_3 in free roll motion. (b) Identification of Γ_6 in free pitch motion.
 (c) Identification of Γ_8 in free yaw motion.

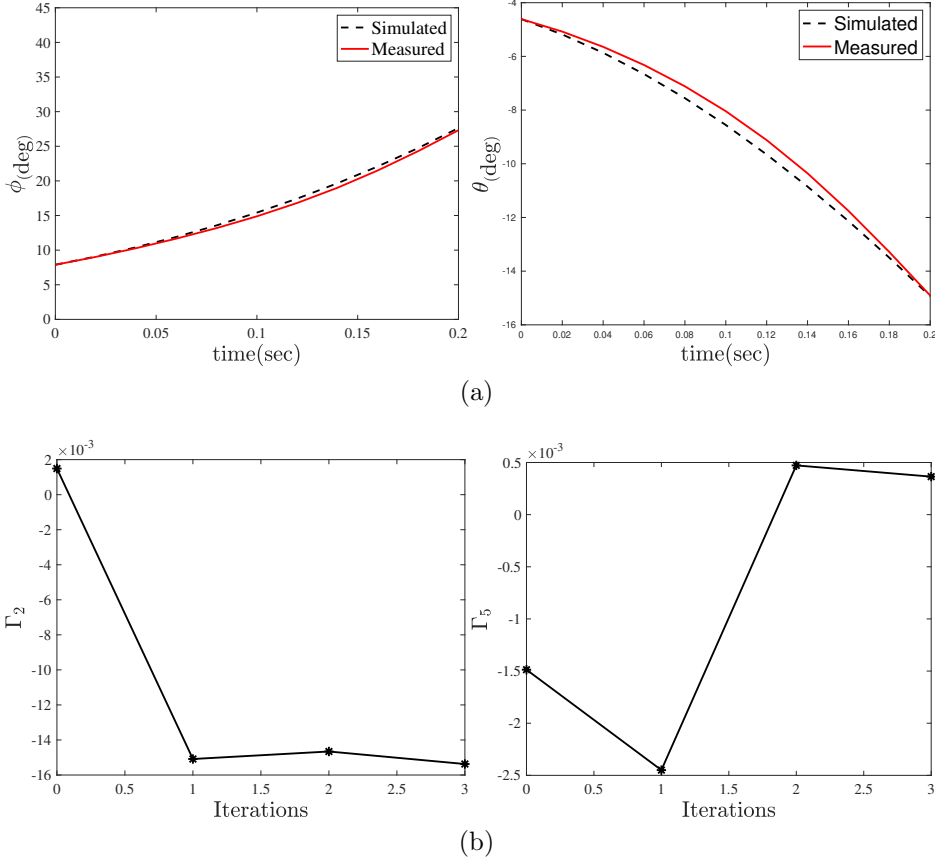


Figure 6: Identification process results when the quadrotor rotates about its roll and pitch axes: (a) Comparison of Simulation and experimental results. (b) Identification of Γ_2 and Γ_5 .

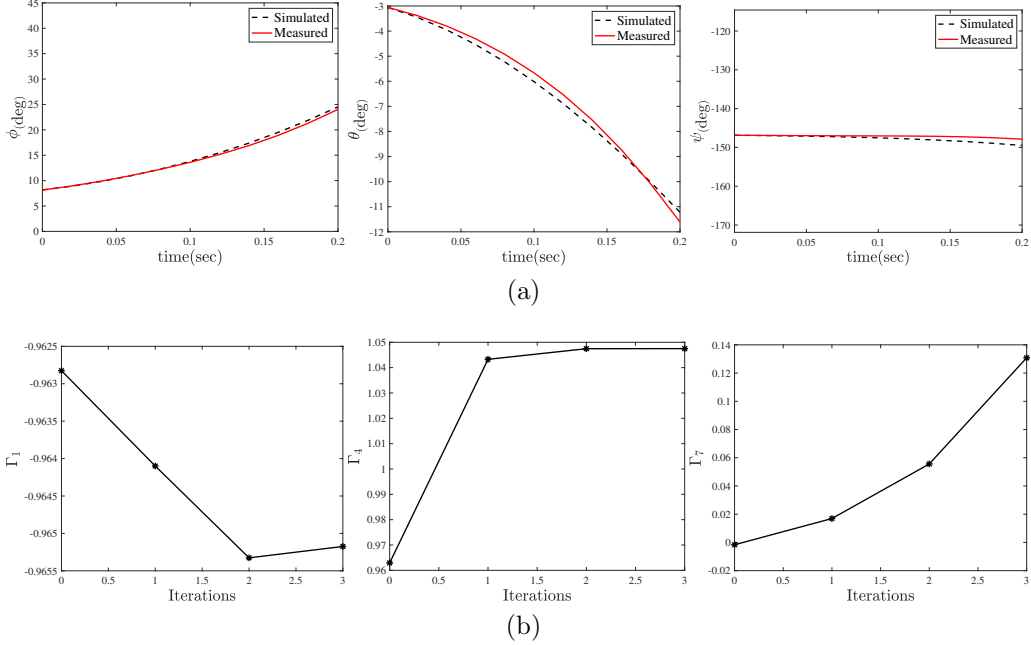


Figure 7: Identification process results when the quadrotor rotates about its roll, pitch, and yaw axes: (a) Comparison of Simulation and experimental results. (b) Identification of Γ_1^{-1} , Γ_4 and Γ_7 parameters.

5.2. Evaluation of LQIR-DG Performance

Here, the performance of the LQIR-DG controller algorithm is evaluated for regulation and tracking performance, disturbance rejection, and the impact of model uncertainty. Finally, the performance of the proposed controller is compared to the PID controller and variants of the LQR controller. The parameters of the PID controller are presented in Table 5.

Table 5: Parameters of PID Controller

Channel	K_p	K_i	K_d
Roll	2.0	0.5	1.0
Pitch	1.5	0.4	0.8
Yaw	3.0	0.6	1.2

5.2.1. Performance of the LQIR-DG Controller

Here, the results of the LQIR-DG controller method are presented for the control loops of the Euler angles of the experimental platform in Figures 8 and 9. The performance of the proposed controller is evaluated in Figure 8. Figure 8 (a) compares the desired and output signals, i.e., the Euler angles during regulation. Figure 8 (b) compares the desired square wave input with a frequency of 0.02 Hz and an amplitude of 20 degrees with the output signals in the two-degree-of-freedom coupling mode. Moreover, Figures 9 (a) and (b) show the rotational velocity command of the quadrotor in the regulation and tracking problems, respectively. These results demonstrate that the roll, pitch, and yaw angles are accurately controlled by the proposed approach.

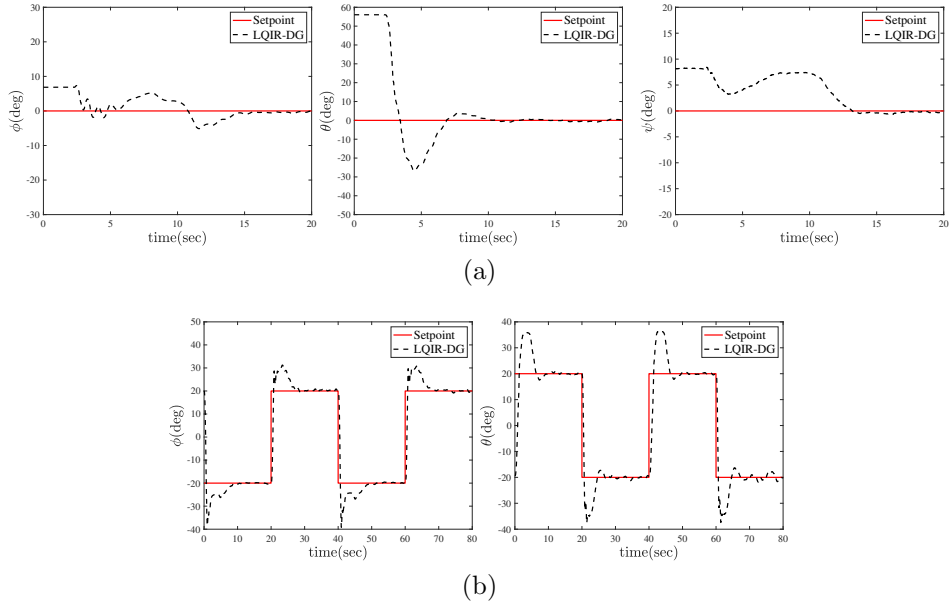


Figure 8: Comparison of Euler angles in (a) regulation (b) Tracking Conditions

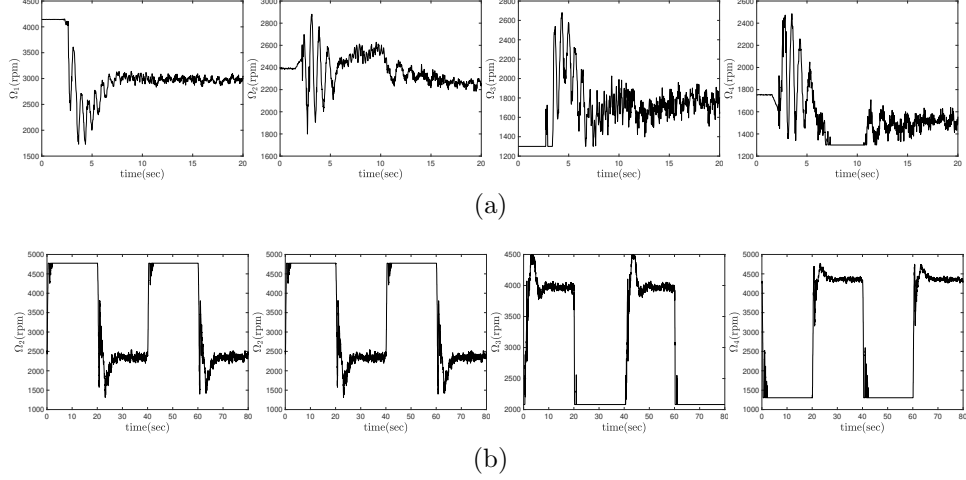


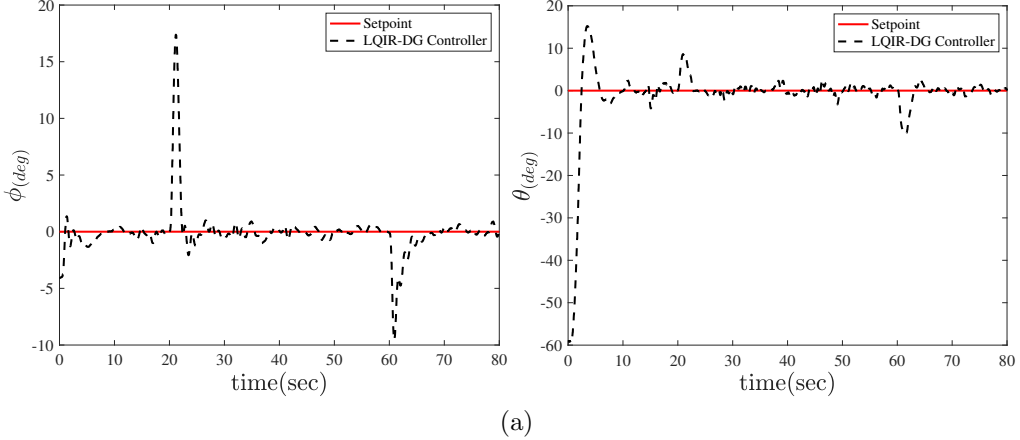
Figure 9: Temporal Evolution of Angular Velocity Commands for the LQIR-DG Controller

5.2.2. Performance of the LQIR-DG in Disturbance Rejection

The performance of the proposed controller in the input disturbance is shown in Figure 10. The input disturbance, $d\Omega_i$, is considered as a change in the command of the rotational velocity, modeled as:

$$d\Omega_1 = d\Omega_2 = -d\Omega_3 = -d\Omega_4 = \begin{cases} 500_{\text{rpm}} & 20 < t < 60 \\ 0 & \text{other} \end{cases} \quad (38)$$

Figure 10 (a) illustrate the desired and the actual roll and pitch angles in the regulation problem. The results indicate that the LQIR-DG controller can stabilize the quadrotor platform when the input disturbance is present.



(a)

Figure 10: Comparison of the desired and actual roll and pitch angle in the presence of the input disturbance.

5.2.3. Investigating the Impact of Modeling Uncertainty

In this section, the performance of the LQIR-DG controller is investigated while considering uncertainty in the 3DoF experimental model. To achieve this, 50 and 100 grams were added to the roll and pitch axes, respectively, as shown in Figure 11. Figure 12 (a) compares the desired and the actual roll angle and Figure 12 (b) shows the desired and the actual pitch angle when the uncertainty of moments of inertia is presented. Moreover, Figure 12 (c) shows the rotational velocity command of the experimental platform in the presence of model uncertainty. The implementation results indicate that the LQIR-DG controller converges to the desired values in the presence of the modeling uncertainty.



Figure 11: Quadrotor 3DoF Platform with Added Weight.

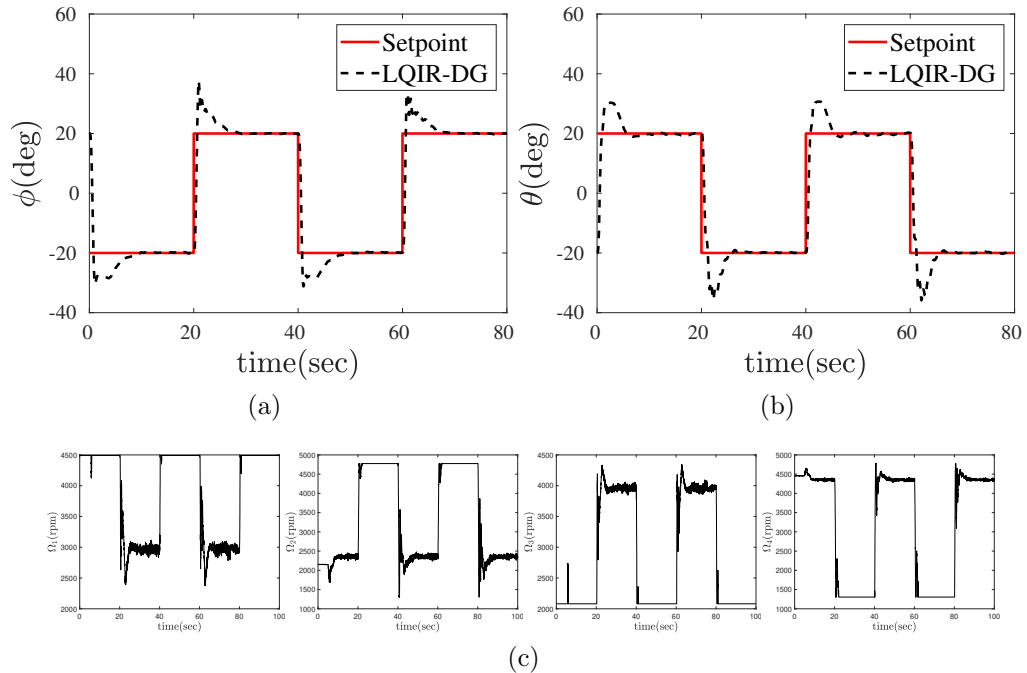


Figure 12: Comparison of the LQIR-DG controller when the uncertainty of moment of inertia is presented

5.2.4. Comparison with the Control Strategies

Here, the LQIR-DG controller performance is compared with the PID controller and variant of the LQR strategies such as the LQR and LQIR in Figure

13. Figure 13 compare the desired and the actual attitude of the quadrotor platform in the presence of these controllers. Moreover, the RSME of the controllers of all the controllers, i.e, boxplot, are compared in Figure 14. The median of RMSE is shown in the crossline in the boxplot.

These results indicate that the LQIR-DG controller is able to provide an excellent transient response and rapid convergence relative to other controllers for attitude control of the quadrotor experimental platform.

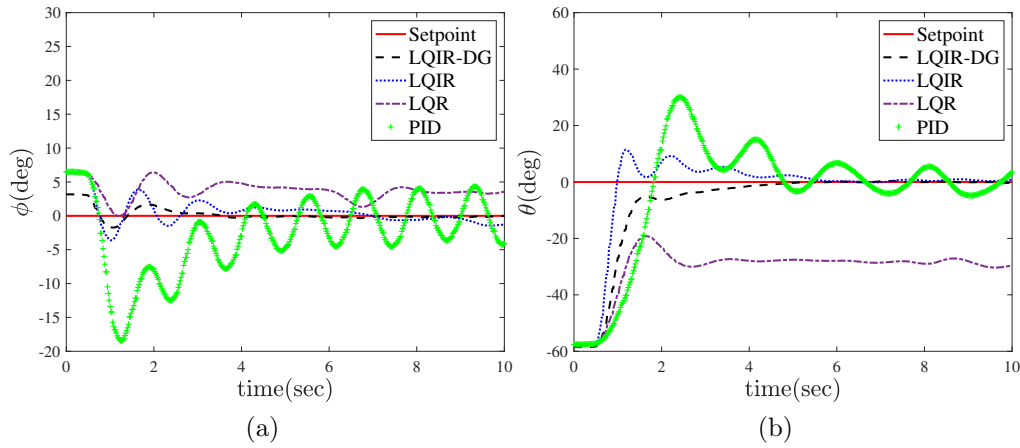


Figure 13: The implementation results of the LQIR-DG Control Strategy with added weight on the roll and pitch axes in the three-degree-of-freedom coupling mode. (a) Comparison of the desired roll angle with the actual roll angle, (b) Comparison of the desired pitch angle with the actual pitch angle.

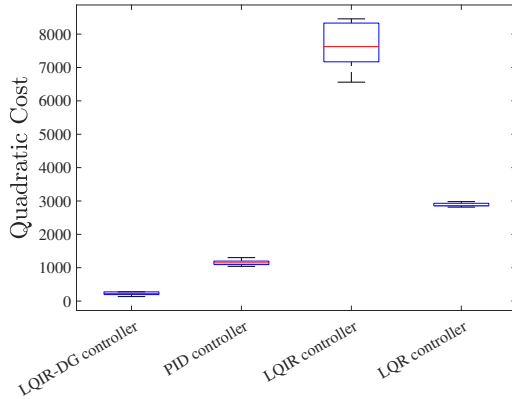


Figure 14: Comparative Analysis of the LQIR-DG Control Strategy versus LQR, LQIR, and PID Controllers using Quadratic Cost Function

6. Conclusion

References

- Bouabdallah, S., 2007. Design and control of quadrotors with application to autonomous flying doi:10.5075/epfl-thesis-3727.
- Bouabdallah, S., Siegwart, R., 2007. Full control of a quadrotor, in: 2007 IEEE/RSJ International Conference on Intelligent Robots and Systems, pp. 153–158. doi:10.1109/IROS.2007.4399042.
- Engwerda, J., 2006. Linear Quadratic Games: An Overview. WorkingPaper. Macroeconomics. Subsequently published in Advances in Dynamic Games and their Applications (book), 2009 Pagination: 32.
- Fathoni, M.F., Lee, S., Kim, Y., Kim, K.I., Kim, K.H., 2021. Development of multi-quadrotor simulator based on real-time hypervisor systems. Drones 5. URL: <https://www.mdpi.com/2504-446X/5/3/59>, doi:10.3390/drones5030059.